A Lagrangian analysis of ice-supersaturated air over the North Atlantic

JOURNAL OF GEOPHYSICAL RESEARCH: ATMOSPHERES, VOL. 119, 90–100, doi:10.1002/2013JD020251, 2014

A Lagrangian analysis of ice-supersaturated air over the North Atlantic

E. A. Irvine,[1] B. J. Hoskins,[1,2] and K. P. Shine[1]

Received 20 May 2013; revised 6 December 2013; accepted 9 December 2013; published 14 January 2014.

[1] Understanding the nature of air parcels that exhibit ice supersaturation is important because they are the regions of potential formation of both cirrus and aircraft contrails, which affect the radiation balance. Ice-supersaturated air parcels in the upper troposphere and lower stratosphere over the North Atlantic are investigated using Lagrangian trajectories. The trajectory calculations use European Centre for Medium-Range Weather Forecasts Interim reanalysis data for three winter and three summer seasons, resulting in approximately 200,000 trajectories with ice supersaturation for each season. For both summer and winter, the median duration of ice supersaturation along a trajectory is less than 6 h. Five percent of air which becomes ice supersaturated in the troposphere and 23% of air which becomes ice supersaturated in the stratosphere will remain ice supersaturated for at least 24 h. Weighting the ice-supersaturation duration with the observed frequency indicates the likely overall importance of the longer duration ice-supersaturated trajectories. Ice-supersaturated air parcels typically experience a decrease in moisture content while ice supersaturated, suggesting that cirrus clouds eventually form in the majority of such air. A comparison is made between short-lived (less than 24 h) and long-lived (greater than 24 h) ice-supersaturated air flows. For both air flows, ice supersaturation occurs around the northernmost part of the trajectory. Short-lived ice-supersaturated air flows show no significant differences in speed or direction of movement to subsaturated air parcels. However, long-lived ice-supersaturated air occurs in slower-moving air flows, which implies that they are not associated with the fastest moving air through a jet stream.

Citation: Irvine, E. A., B. J. Hoskins, and K. P. Shine (2014), A Lagrangian analysis of ice-supersaturated air over the North Atlantic, *J. Geophys. Res. Atmos.*, *119*, 90–100, doi:10.1002/2013JD020251.

1. Introduction

[2] The upper troposphere contains regions of ice supersaturation (ISS), where the relative humidity with respect to ice is above 100%, and the temperature is usually defined to be less than 235 K to identify only regions of ice phase and not mixed phase [*Pruppacher and Klett*, 1997]. These regions are interesting for two reasons. First, given sufficiently high supersaturations, regions of ISS support the formation of natural cirrus clouds by homogeneous freezing or in some cases heterogeneous freezing [e.g., *Hoose and Möhler*, 2012]. Second, the occurrence of ice-supersaturated regions in the upper troposphere and lower stratosphere coincides with the cruising altitude of commercial aircraft; aircraft flying through these regions may form persistent contrails which may have a relatively large, if uncertain, impact on climate [*Lee et al.*, 2009; *Burkhardt and Kärcher*, 2011]. A mean ISS of 15% has been observed in ice-supersaturated air in the upper troposphere [*Gierens et al.*, 1999]; this is below the threshold for homogeneous freezing, and therefore, persistent contrails may form in ice-supersaturated air that is free of natural cirrus cloud.

[3] The global distribution of ice-supersaturated regions (ISSRs) can be derived from satellite data, which show that globally, the maximum frequency of occurrence is in the tropics, where it is related to the occurrence of deep convection. Tropical ISSRs are not considered in this paper, as they typically occur at altitudes higher than aircraft cruise altitudes. In the midlatitudes, high frequencies of supersaturation are coincident with the storm track [*Spichtinger et al.*, 2003; *Lamquin et al.*, 2012]. ISSRs have also been diagnosed using meteorological analyses, and their location linked to synoptic features. Using this method, ISSRs have been found to preferentially occur in high pressure regions [*Immler et al.*, 2008; *Gierens and Brinkop*, 2012], in association with jet stream circulations [*Irvine et al.*, 2012] and in warm conveyor belts associated with midlatitude cyclones [*Spichtinger et al.*, 2005a]. Generally, ISSRs occur in air that has experienced large-scale upward and often divergent motion [*Kästner et al.*, 1999; *Gierens and Brinkop*, 2012] and are thus both cooler and

[1]Department of Meteorology, University of Reading, Reading, UK.
[2]Grantham Institute for Climate Change, Imperial College London, London, UK.

Corresponding author: E. A. Irvine, Department of Meteorology, University of Reading, Earley Gate, Reading RG6 6BB, UK. (e.a.irvine@reading.ac.uk)

2169-897X/14/10.1002/2013JD020251

moister than surrounding subsaturated air [*Gierens et al.*, 1999; *Spichtinger et al.*, 2003].

[4] The location and duration of ISSRs are controlled by and evolve with the synoptic flow. ISSRs identified from observations or synoptic charts give us an Eulerian view of ice supersaturation. However, ISSRs are dynamic features—air flowing through a synoptic pattern forms part of the ISSR when it becomes saturated and remains part of the ISSR only while saturated (this perspective is discussed in *Spichtinger et al.* [2005a] and *Schumann* [2012]). Therefore, the timescales of an ISSR and an ice-supersaturated air parcel are different, making it difficult to diagnose from a synoptic chart how long an air parcel will remain ice supersaturated, which is an important consideration if contrails form within this air parcel. Contrails formed in cold ice-supersaturated air are advected with the air parcel through a weather pattern and may last for many hours; contrail cirrus outbreaks have been observed to persist for 12–18 h [*Minnis et al.*, 1998; *Duda et al.*, 2004; *Haywood et al.*, 2009].

[5] The dynamic nature of ISSRs lends itself to an alternative approach for analyzing these regions, by using Lagrangian trajectories. This approach has previously been applied to two case studies of ISS over Germany [*Spichtinger et al.*, 2005a, 2005b] and for a cirrus cloud in an ISSR [*Montoux et al.*, 2010]. Here we extend this approach by using trajectories to characterize air flows which lead to ISS in the North Atlantic region over multiple seasons. We focus on understanding long-lived ice-supersaturated air flows, which may be most important to understand from a radiative perspective as they can support long-lived persistent contrails and also natural cirrus clouds.

[6] The method for the calculation of the Lagrangian trajectories and that used to identify ice-supersaturated air are presented in section 2 together with an example for a synoptic situation with strong ridging over the North Atlantic. Properties of the ice-supersaturated air parcels are analyzed in section 3.1, including the duration of ISS, the spatial distribution of ISS, and the evolution of moisture along the trajectory. Differences between air parcels which have long duration and short duration ISS, such as their direction and speed of movement, are analyzed in section 3.2, and conclusions are presented in section 4.

2. Methodology

2.1. Description

[7] Fully Lagrangian trajectories are calculated using an offline trajectory model [*Methven*, 1997; *Jackson et al.*, 2001], where the term offline means that the wind fields are obtained directly from reanalysis data. The Lagrangian code uses a fourth-order Runge-Kutta integration with a 1 h time step to calculate the trajectories. The horizontal wind fields used to advect the air parcel are taken from the reanalysis data, and the vertical velocity is calculated using the continuity equation. Once the position of an air parcel is calculated, the gridded reanalysis data are then interpolated to the current trajectory location. The accuracy of the trajectory model has been examined for the extratropics in *Methven et al.* [2003] and for the tropics in *Cau et al.* [2005].

[8] The input meteorological data are 6-hourly European Centre for Medium-Range Weather Forecasts Interim reanalysis data (ERA-Interim) [*Dee et al.*, 2011] with horizontal resolution T255 and 60 vertical levels. The parameterization of homogeneous nucleation and ice supersaturation in the model cloud scheme are described in *Tompkins et al.* [2007]. In summary, the relative humidity over ice in the clear-sky portion of a grid box is allowed to increase above 100%, up to a critical threshold. On reaching this threshold, excess humidity is converted to ice and the in-cloud humidity adjusted back to 100%, within the model time step.

[9] Trajectories are released within the North Atlantic, defined to be the area 35°N–75°N, 0°W–70°W (shown on Figure 1a), on a grid with 1° horizontal spacing and from three pressure levels: 300 hPa, 250 hPa, and 200 hPa. We will refer to the time the trajectories are initialized as $t = 0$. From this grid, trajectories are calculated forward in time to $t + 48$ h and backward in time to $t - 48$ h, giving a complete trajectory length of 96 h.

[10] Trajectories are initialized every 12 h during three winters (December, January, and February) and three summers (June, July, and August). The winters (starting December 1994, 1995, and 2003) and summers (1994, 1998, and 2006) were chosen for their different North Atlantic Oscillation [*Barnston and Livezey*, 1987] behavior, in order to capture a range of synoptic conditions over the North Atlantic. In total, the number of trajectories calculated per season exceeds 4.6 million.

[11] We use both relative humidity and temperature criteria to determine whether an air parcel is within a region of ice supersaturation. A criterion that the relative humidity with respect to ice is above 98% is used. We take a threshold below 100% for two reasons. First, given the relatively coarse resolution of the ERA-Interim data, a grid box with a grid mean humidity slightly below 100% is likely to contain some air parcels with humidity above 100%; thus, a threshold of 98% accounts for this subgrid-scale variability. The second reason is to account for a bias from recalculating the relative humidity from its temperature and moisture fields, which is introduced by data interpolations onto different grids (P. Berrisford, personal communication; European Centre for Medium-Range Weather Forecasts (ECMWF), 2012). In addition, consistent with previous studies of ISS, we apply the criterion that the temperature should be below 235 K to avoid identifying mixed-phase regions [*Pruppacher and Klett*, 1997]. The results presented in this paper have been recalculated with humidity thresholds of 95% and 100% and found to be qualitatively similar. The main effect of using a modified humidity threshold is on the number of ISS trajectories identified; for a threshold of 95% there is also a 6% increase in the proportion of ISS trajectories with ISS duration of at least 24 h.

[12] In this study we do not consider separately clear-sky and cloudy trajectories, since the trajectories are calculated offline, and the information allowing us to distinguish such trajectories is not available in the ERA-interim output. Interpolating a discontinuous field such as cloud cover onto trajectories is problematic, and we do not attempt to do so. We note, however, that it is rare for trajectories to have achieved saturation with respect to liquid water in the 18 h preceding them becoming ice supersaturated. In the one winter for which we assessed this, fewer than 1% of

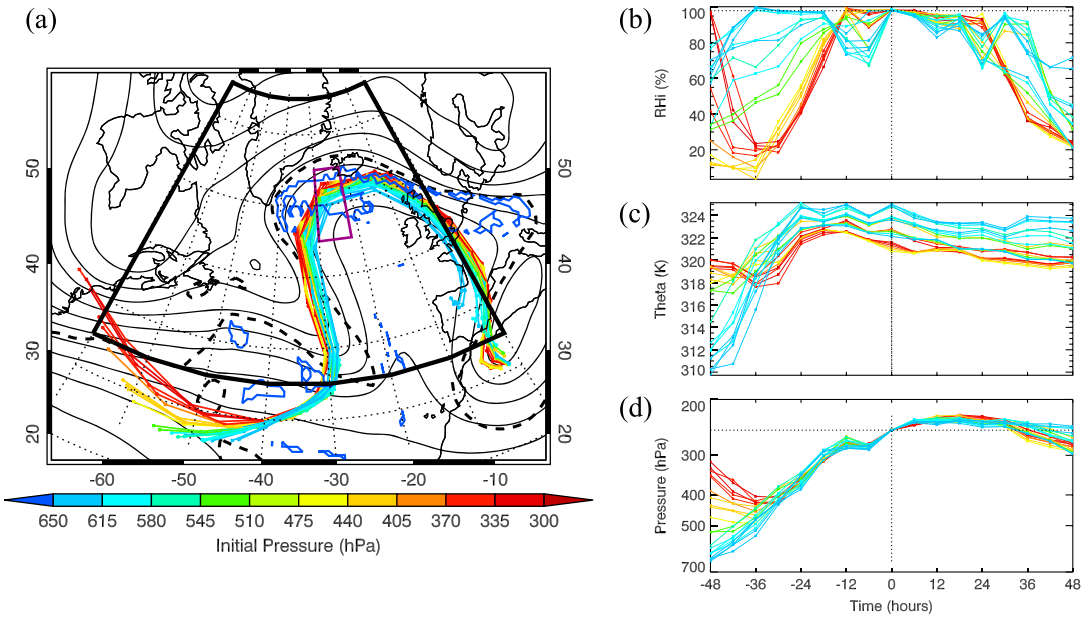

Figure 1. (a) An example of trajectories initialized within the purple box at 250 hPa; only trajectories which were within the ice-supersaturated region within this box (blue contours) are shown. The trajectories are released at $t = 0$, corresponding to 1800 UTC 19 January 2004. The synoptic pattern at this time is shown by the 250 hPa geopotential height (thin black contours); the dynamical tropopause is displayed using the 2 PVU contour (thick dashed black line); and regions of ice supersaturation at 250 hPa are outlined in blue. The path of the ISS trajectories is shown from $t-48$ to $t+48$, colored by the pressure of the air at $t-48$. The black box defines the North Atlantic region that the trajectories used in this study were initialized in. For the same period, (b) the relative humidity calculated with respect to ice, (c) potential temperature (theta), and (d) pressure along the trajectories.

trajectories attained a relative humidity of 80% with respect to liquid water (the threshold for stratiform liquid water cloud formation in the ECMWF model [*Tiedtke*, 1993]) prior to attaining ice supersaturation.

[13] Trajectories are released from multiple pressure levels. This could lead to a double counting of trajectories which rise from one level to another while the air is ice supersaturated. Occurrences of trajectories ascending from 300 to 250 hPa or 250 to 200 hPa while ice supersaturated were found in fewer than 0.2% of winter trajectories. We therefore assume this to have a negligible effect on our results. A second possibility, arising from releasing trajectories every 12 h, is double counting of trajectories where the duration of ISS along the trajectory is greater than 12 h. To avoid double-counting ISS trajectories, we consider only those trajectories which meet the criteria for ISS at the initial time ($t = 0$). These trajectories are referred to as ISS trajectories; trajectories which do not meet this criteria are considered as subsaturated trajectories (even if the criteria are met at other points along the trajectory). Applying the above criteria results in a total of 249,874 ISS trajectories in the winter data and 188,895 in the summer data.

[14] In our results we have divided the ISS trajectories into tropospheric and stratospheric. Ice supersaturation has been observed to occur in the lower stratosphere near the tropopause [*Gierens et al.*, 1999]. However, the ISS in these regions is associated with low temperatures and very low specific humidities compared to such regions in the troposphere [*Spichtinger et al.*, 2003], and therefore, the size of the radiative effect of contrails which form in these regions is uncertain. In this study, a dynamic tropopause definition of 2 potential vorticity units (PVU) is used, which is appropriate for the range of latitudes considered. We defined tropospheric ice-supersaturated air to be trajectories where the first point of ISS is within the troposphere (i.e., the potential vorticity at this point is less than 2 PVU) and similarly for stratospheric air. In winter ice supersaturation occurs on 3.3% of stratospheric trajectories (1.6% for the summer data) which agrees well with *Gierens et al.* [1999] who found ice supersaturation in 2% of stratospheric data. Similarly, ice supersaturation occurs on 9.5% of tropospheric trajectories in winter and 7% in summer. Because stratospheric ice-supersaturated air is often located close to the tropopause, the partitioning of ISS air into tropospheric and stratospheric has some sensitivity to the tropopause definition, particularly at high latitudes. It could be argued that a higher threshold of 3 PVU or above may be preferable to define the tropopause at high latitudes [*Zängl and Hoinka*, 2001]; here we used a single tropopause definition, and note that using a tropopause definition of 3 PVU for the region north of 60°N reduces the amount of ice-supersaturated air identified as stratospheric over Greenland.

2.2. Illustrative Case Study

[15] As an illustration of the method used, we present a case study of trajectories initialized within an ISSR. The

synoptic pattern at 250 hPa is shown at $t = 0$ (Figure 1a), corresponding to 1800 UTC 19 January 2004, when the trajectories were released. At this time, there is strong ridging over the eastern North Atlantic, with a large region of ISS just below the tropopause around the northern edge of the ridge. The 21 trajectories displayed in Figure 1 originated at 250 hPa from within this region of ISS (and within the purple box on Figure 1a). The trajectories can be split into two broad groups according to their pressure at $t - 48$ h: one starting around 350 hPa (mostly the red trajectories on Figure 1) and initially moving southward and eastward and one starting around 600 hPa (mostly the blue trajectories in Figure 1) and ascending as they move northward and eastward. Air moving northward would be expected to ascend along isentropic surfaces; the increase in potential temperature (Figure 1c), accompanied by a decrease in specific humidity from 4 g kg^{-1} to 0.5 g kg^{-1} (not shown), suggests release of latent heat from condensation into cloud droplets during this ascent (note that clouds form when the relative humidity criteria is reached locally, as defined by the parameterization of the subgrid-scale variability, and therefore, cloud formation may occur when the grid-mean humidity is substantially below the critical value [*Tompkins et al.*, 2007]). The ascent around the ridge cools the air, leading to an increase in relative humidity (Figure 1b), and the air attains ISS around the top of the ridge and remains ISS until the air is forced to descend (Figure 1d) as it begins to move southward and warms. The small decrease in potential temperature, of 1 K day^{-1}, (and negligible change in specific humidity, not shown) while the air is supersaturated and in the upper troposphere, is consistent with typical radiative cooling rates. The time from the beginning to the end of the trajectories is 96 h, showing that the large-scale synoptic trough-ridge pattern persisted during this time. In this particular case study, the air only just attains ice supersaturation; however, high ice supersaturations of up to 140% are observed in other cases.

[16] The dynamic nature of ISSRs and the air which makes up these regions is illustrated by considering their respective durations. The duration of ISS of an air parcel is defined as the time period during which the air parcel is continually ice supersaturated; the precision of the calculation is therefore limited by the 6 h time resolution of the meteorological data. For example, an air parcel which is ice supersaturated at a single point, $t = 0$, along a trajectory could be supersaturated for less than a single hour or just under 12 h (if it becomes saturated just after $t - 6$ and becomes subsaturated just before $t + 6$). This is likely to result in an overestimate of the duration; therefore, we take the minimum possible time as the duration of ice supersaturation: ISS at a single point is given a duration of less than 6 h, at two consecutive points a duration of 6 h, at three consecutive points a duration of 12 h, and so on. Using this definition, for this case study, the duration of ISS of the individual air parcels ranges from less than 6 h (17 trajectories) to 12 h (1 trajectory), although many remain close to saturation for 18 h; this is considerably less than the duration of the ice-supersaturated region associated with the ridge. This region of ISS was evident during the 4 days, 17–21 January 2004, that the ridge itself persisted for and disappeared only when the amplitude of the ridge had substantially decreased (not shown).

3. Results

3.1. Properties of ISS Trajectories

[17] In this section the properties of the ISS trajectories, calculated for the three winters and three summers discussed in section 3, will be presented. Three properties are examined: the duration of ISS of an air parcel, the spatial distribution of ISS, and the evolution of key variables while the air is ice supersaturated.

[18] A contrail formed in an ISS air parcel will be advected with the flow in that air parcel (We assume any vertical motion of the contrail associated with falling ice crystals will be small.), and therefore, the duration of ISS is an upper bound on the lifetime of a persistent contrail. The duration of ISS along a trajectory is calculated by considering the number of consecutive points of ISS along the trajectory, where the first point is obtained by searching back in time from $t = 0$ and the end point by searching forward in time from $t = 0$. This definition requires both relative humidity and temperature criteria to be met. Note that a contrail, once formed, requires only the condition of relative humidity to persist. Removing the temperature criterion did not significantly change the calculated ISS durations.

[19] The time resolution of the meteorological data used in the trajectory calculations is 6-hourly, which is insufficient to accurately determine the period for which an air parcel is ice supersaturated. It does, however, allow some general conclusions to be drawn. Probability density functions (Pdfs) of the duration of ISS air (Figure 2) are non-Gaussian and highly skewed toward shorter durations. The median duration is less than 6 h, i.e., ice supersaturation was only observed at a single point along the trajectory (at $t = 0$). This is true for air parcels in both summer and winter. The shape of the pdf is in agreement with previous studies of the lifetime of satellite-observed linear contrails [*Vazquez-Navarro*, 2009], although we note that the tail of the distribution is longer here than in *Vazquez-Navarro* [2009] probably because the method detects contrails only while linear features and not once they have spread into contrail cirrus. It is also in agreement with the lifetime of modeled contrails [*Schumann*, 2012], though care must be taken in the comparison since in *Schumann* [2012] the lifetime of contrails is limited by sedimentation. Note that the lifetime of contrails is generally smaller than that of the ice-supersaturated air parcel they form in, since as noted by *Schumann* [2012] the air parcel must become saturated and then an aircraft must fly through it to form the contrail. In addition loss processes, such as the sedimentation of ice particles, may reduce the contrail optical depth leading to a subvisible contrail, before the subsaturation of the ambient ice-supersaturated air.

[20] The pdfs of ISS durations have a different shape for air which becomes ice supersaturated in the troposphere and air which becomes ice supersaturated in the stratosphere. In winter, air which becomes ice supersaturated in the stratosphere has a median duration of 6 h compared to less than 6 h for tropospheric ISS air. A greater proportion of stratospheric ISS air, 23% compared to 5% for tropospheric air, has a duration of ISS of at least 24 h. In summer the difference is reduced; 11% of stratospheric ISS air and 5% of tropospheric ISS air have an ISS duration of at least 24 h. As noted in section 2.1, the partitioning of ISS trajectories into

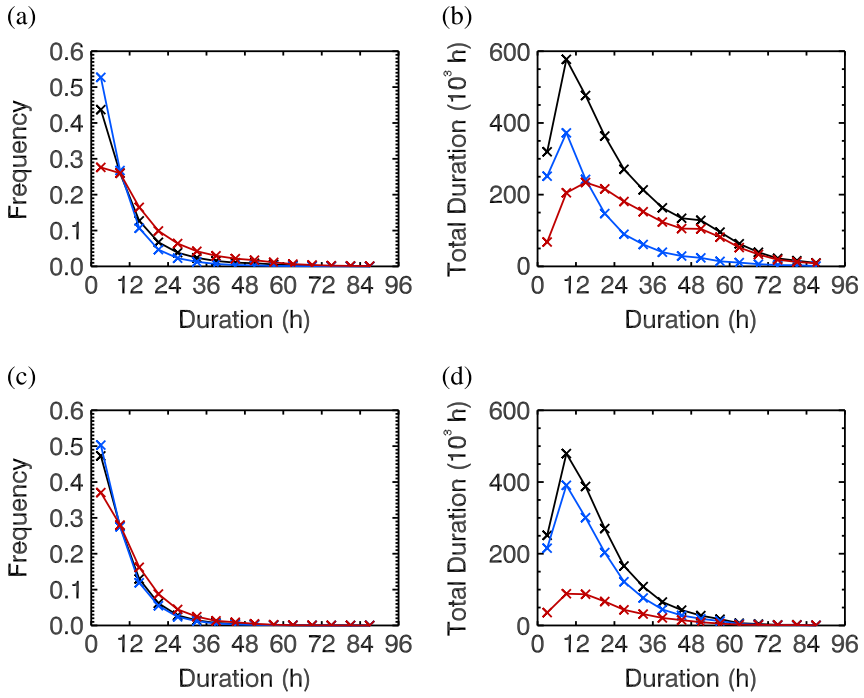

Figure 2. Histograms of the duration of ice-supersaturation calculated along air parcel trajectories, for trajectories released from all three pressure levels for (a) all three winters and (c) all three summers, using duration bins of 6 h. The three lines correspond to all ISS trajectories (black), tropospheric ISS air (blue) and stratospheric ISS air (red). Histograms of the total duration in units of 10^3 h, calculated for each duration bin as the median duration multiplied by the number of trajectories with that duration, (b) for winter and (d) for summer.

tropospheric and stratospheric is sensitive to the tropopause definition; however, we note that the proportion of ISS trajectories with a lifetime of at least 24 h is increased by only a few percent if a tropopause definition of 3 PVU is used instead of the 2 PVU definition used here.

[21] A contrail formed in an air mass for which the ISS duration is t_i is likely to persist for a time of order t_i. If we consider that a longer-lived ISS air parcel is more likely to have (a) an aircraft fly through it and that (b) a contrail formed within it will evolve into contrail cirrus, then it is useful to have a measure of the overall longevity of each lifetime category. This is calculated as $N_i t_i$, where N_i is the number of trajectories of a given duration (from Figures 2a and 2c). Since the units are time, we refer to this measure as the total duration. The total duration is shown in Figures 2b and 2d. The shortest (0–6 h) ISS duration, although the most frequent, does not contribute as much to the total duration of ISS air as ISS trajectories which have a duration of 12 h. The importance of stratospheric ISS air is also evident; the total duration of stratospheric ISS air is larger than that of tropospheric ISS air for durations greater than 18 h in winter. This shows that the contribution of stratospheric ISS air may be significant, if contrails were to form in it, because of its longer total duration, although other factors such as the temperature, available moisture, and natural cloud cover are also important in determining the radiative effect of such contrails. However, in summer the proportion of ISS air in the stratosphere is much smaller than in the troposphere due to both warmer air and a higher tropopause; therefore, tropospheric ISS air has a much greater total duration than stratospheric ISS air. Figure 2 shows that the total duration of longer-lived ISS air is significant and hence may be important in determining the contrail forcing. We will therefore give particular attention to those ISS trajectories which have a long duration, defined here as continuous ice supersaturation for at least 24 h, under the assumption that these may be the most important to understand.

[22] The spatial distribution of the ISS start points, the location of air when it becomes ice supersaturated, is shown in Figure 3 for trajectories released on all three levels, for all 3 years of data. The outline of the North Atlantic region that the trajectories were initialized in is clearly visible, due to the short duration of ISS along most of the trajectories (Figure 2), so to first order Figure 3 shows the actual distribution of ISS in the upper troposphere within this region. The distribution of ISS compares well to previous studies [*Spichtinger et al.*, 2003; *Lamquin et al.*, 2012; *Irvine et al.*, 2012]. The distribution of ISS start points in the troposphere in winter and summer is linked to the position of the jet stream, which is generally further north in summer. For stratospheric ISS trajectories, there is a maximum over Greenland in winter, which is largely absent in summer when the higher tropopause results in a smaller proportion of ISS air in the stratosphere at the levels used in this study. There is a northward shift in the position of tropospheric ISS trajectories from winter to summer, which may be caused by both temperatures rising above the threshold used to avoid identifying regions of mixed phase and a northward shift in the jet stream. The spatial distribution of long-lived ISS air is broadly similar to that of all ISS air for tropospheric ISS

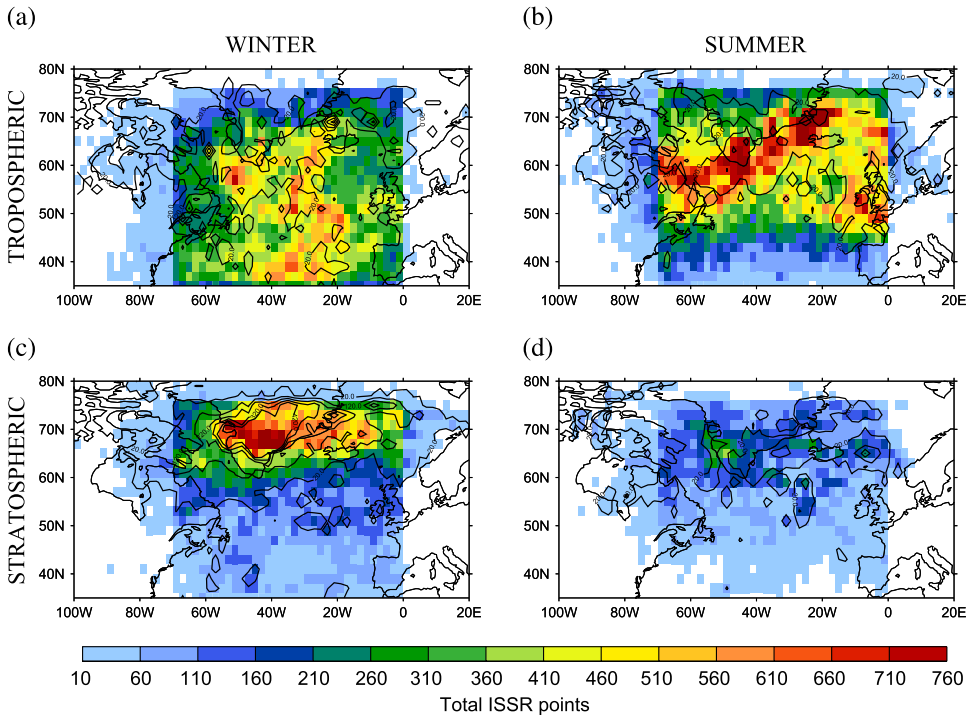

Figure 3. Map of the density of points where air first becomes ISS along a trajectory for all trajectories (colors) and long-lived ISS air (black contours) for (a) tropospheric winter, (b) tropospheric summer, (c) stratospheric winter, and (d) stratospheric summer trajectories. Data have been gridded into 2° boxes before plotting. The minimum values of the line contours for long-lived ISS air is 20 with an interval of 100 trajectories.

air in both seasons, although fewer are associated with the jet stream (Figure 3a).

[23] The Lagrangian trajectories can be used to analyze the evolution of the moisture content, pressure, and temperature of an air parcel, to determine which has a greater control on the duration of ISS. Previous studies have shown that adiabatic cooling of rising air is the main pathway to ISS [*Gierens et al.*, 1999; *Spichtinger et al.*, 2005a], but it is unclear whether it is a decrease in specific humidity from the formation and sedimentation of ice crystals or adiabatic compression of sinking air that have the biggest effect on the duration of ISS. First, we analyze the evolution of the specific humidity of ice-supersaturated air. Pdfs of the change in specific humidity and pressure during the period of ISS are shown in Figure 4, for trajectories where ISS is observed at a minimum of two consecutive points along the trajectory (corresponding to a duration of at least 6 h). Specific humidity decreases by up to 80% during the ISS duration (Figure 4a), while the air undergoes weak ascent of typically less than 20 hPa (Figure 4b) at the same time. The decrease in specific humidity during the period of ISS is consistent with condensation processes from cloud formation, which suggests that cirrus cloud eventually forms in the majority of air masses that become ice supersaturated, although we lack the relevant model data to confirm this. This would agree with lidar observations of ice-supersaturated regions

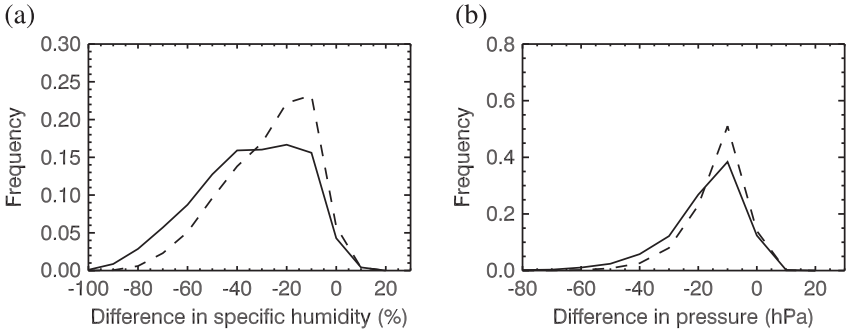

Figure 4. Change in (a) specific humidity and (b) pressure between the last point of ISS and first point of ISS along ISS trajectories released from 250 hPa in winter (solid line) and summer (dashed line). Negative changes in specific humidity indicate drying, and negative changes in pressure indicate ascent during the period of ISS.

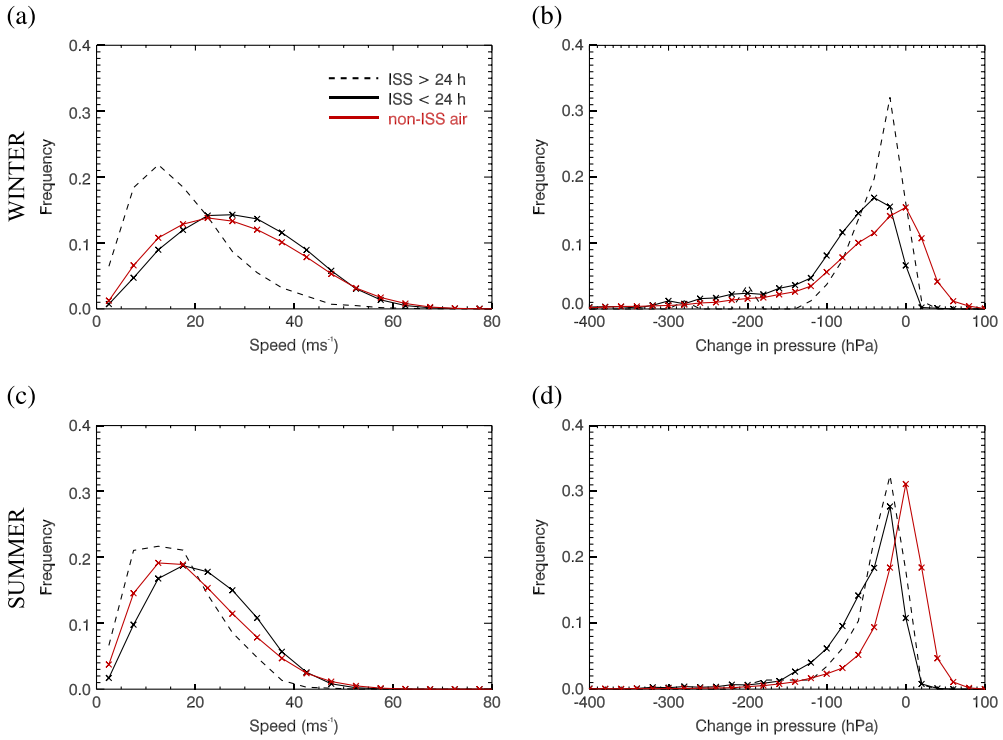

Figure 5. For the 24 h period prior to air becoming ISS, (a) the speed of air and (b) the change in pressure along the trajectory, for winter trajectories, released from all three levels. (c) The speed of air and (d) the change in pressure along the trajectory for summer trajectories. Change in pressure calculated as the pressure at the time the air parcel becomes supersaturated minus the pressure 24 h prior to this. Negative values imply parcel ascent. Shown for: tropospheric ISS air with a lifetime less than 24 h (solid black line), tropospheric ISS air with a lifetime of at least 24 h (dashed black line), and subsaturated air (red line).

which show the majority of ice-supersaturated air also contains ice particles [*Immler et al.*, 2008], so that contrails are often observed embedded in thin or subvisible cirrus [*Immler et al.*, 2008; *Voigt et al.*, 2010; *Iwabuchi et al.*, 2012]. To assess the importance of the changes in specific humidity on the duration of ISS, we recalculated the relative humidity at the first point of subsaturation after the period of ISS, using (1) the specific humidity from the last point of ISS and (2) the pressure and temperature from the last point of ISS, for winter trajectories released from 250 hPa. For case (2) 60% of trajectories are now ISS, whereas for case (1) only 30% of trajectories are ISS. This suggests that adiabatic compression of sinking air parcels is the major control on the duration of ISS of an air parcel.

3.2. A Comparison of Short- and Long-Duration ISS Air

[24] In this section the recent history of air parcels is considered to determine differences between airflows which lead to ice supersaturation and those which do not. Differences between the recent history of long-duration (at least 24 h) ISS air and shorter-duration (less than 24 h) ISS air are also investigated to understand whether it might be possible to know a priori whether an air parcel will remain in an ice-supersaturated state for a significant period of time. This is important to understand from the perspective of the formation of long-lived contrails in such air parcels and their possible evolution into contrail cirrus.

[25] The 24 h period leading up to ISS (or the 24 h period prior to $t = 0$ for subsaturated air) is used to investigate the recent history of supersaturated and subsaturated air masses. Three variables are analyzed: the speed of air and the change in pressure along a trajectory and the direction of movement. The speed of air along a trajectory is the wind speed in the region of the trajectory, since the trajectories are calculated by using the horizontal wind components to advect air parcels. Equally, the change in pressure along the trajectories is the vertical motion of the ambient air, with negative values implying ascent. Pdfs of wind speed and vertical motion are shown in Figure 5, for both ISS air and subsaturated air, which is used as a climatology. In winter (Figure 5a), the speed of subsaturated air has an approximately normal distribution, with a peak around 30 m s^{-1} and a tail out to 70 m s^{-1} indicative of air flowing through the jet stream. The pdf for shorter-lived ISS air is almost identical to subsaturated air. In contrast, for long-lived ISS the distribution is highly skewed toward smaller speeds with a peak at around 10 m s^{-1}. In summer (Figure 5c), the distribution of the speed of subsaturated air peaks at lower speeds of around 20 m s^{-1}, and the tail cuts off at smaller speeds than in winter. As for winter, long-lived ISS air is associated with smaller wind speeds than shorter-lived ISS air, although the difference is less pronounced, due to the smaller range of

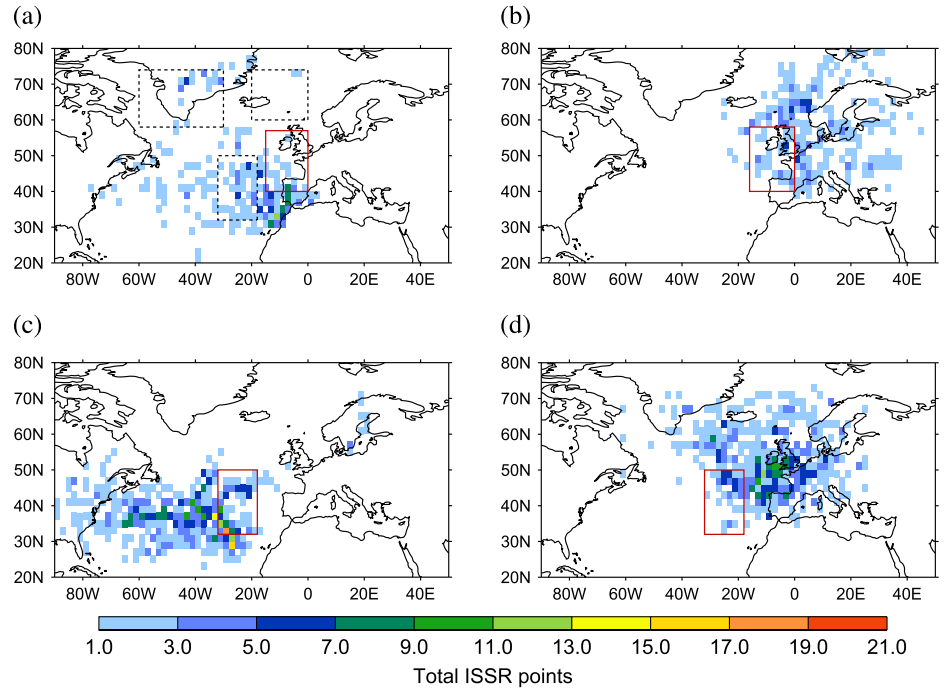

Figure 6. For ISS trajectories released from all levels in winter, whose the first point of ISS is within the Atlantic-European region (defined by the red box, top row) or Mid-Atlantic region (bottom row), a density map of the location of this air (a and c) 24 h prior to, and (b and d) 24 h subsequent to this time. For tropospheric ISS air with an ISS lifetime of at least 24 h. The locations of all regions are marked as boxes in Figure 6a.

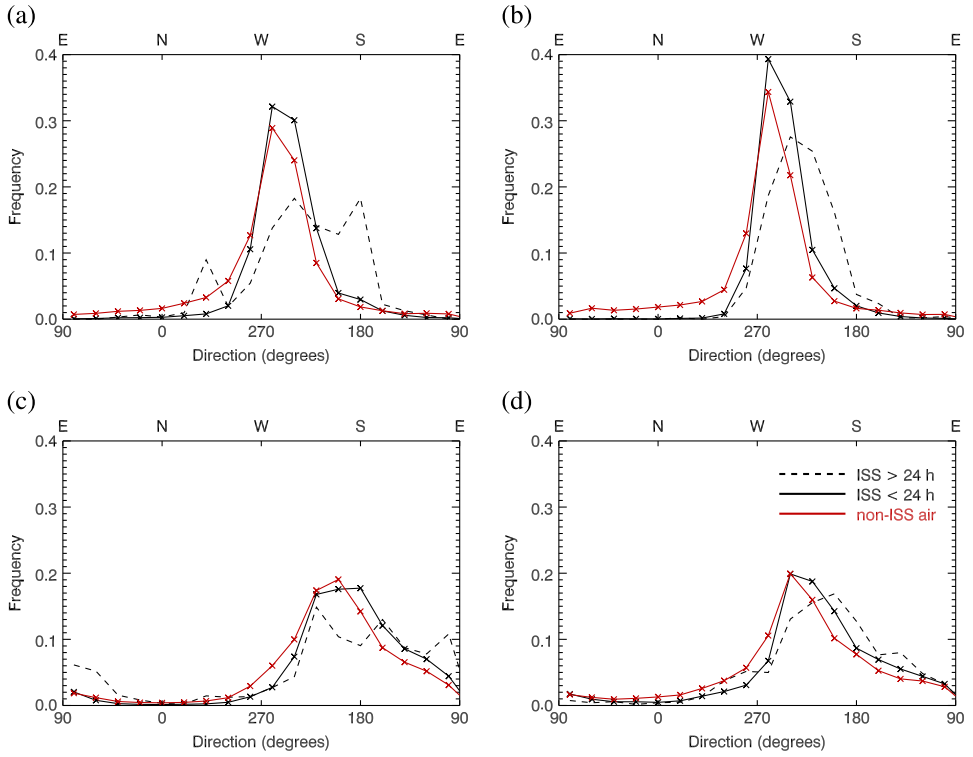

Figure 7. The direction of movement of air along a trajectory in the 24 h leading up to ISS, for regions (a) Atlantic-Europe in winter, (b) Mid-Atlantic in winter, (c) Greenland in winter, and (d) Iceland in summer, for trajectories released from all three levels. Shown for tropospheric ISS air with a lifetime less than 24 h (solid black line), tropospheric ISS air with a lifetime of at least 24 h (dashed black line), and subsaturated air (red line).

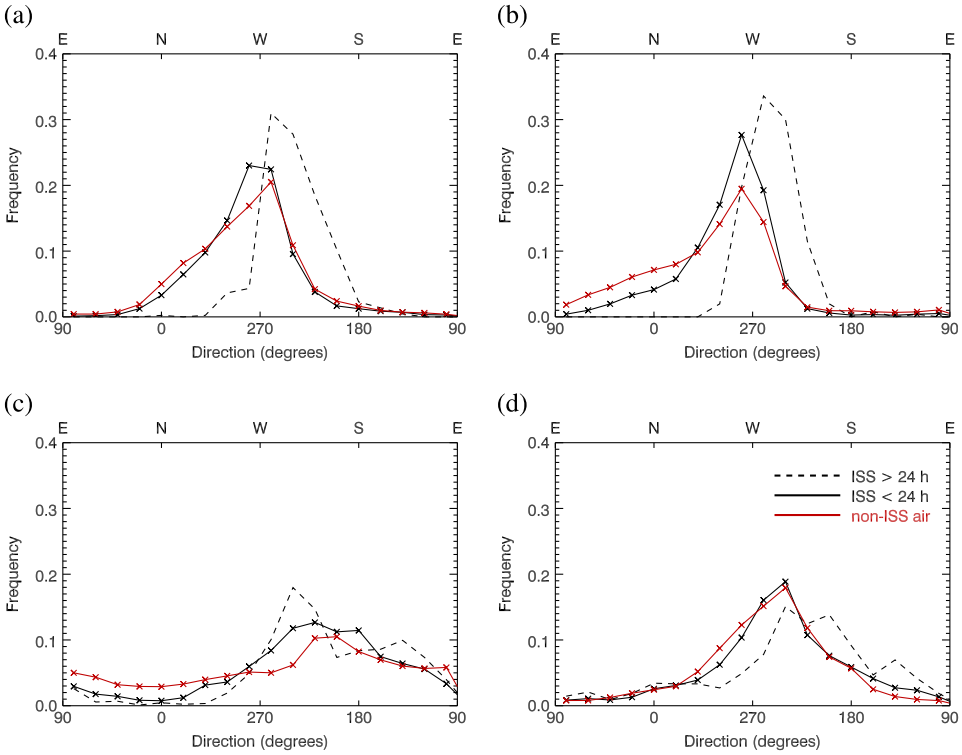

Figure 8. The direction of movement of air along a trajectory in the 24 h following the first point of ISS, for regions (a) Atlantic-Europe in winter, (b) Mid-Atlantic in winter, (c) Greenland in winter, and (d) Iceland in summer, for trajectories released from all three levels. Shown for tropospheric ISS air with a lifetime less than 24 h (solid black line), tropospheric ISS air with a lifetime of at least 24 h (dashed black line), and subsaturated air (red line).

wind speeds observed at these altitudes in summer when the jet stream is weaker.

[26] The distribution of the change in pressure along a trajectory peaks around zero for subsaturated air and contains both ascent and descent. In contrast, while pdfs for both long- and short-lived ISS air have a peak near zero ascent, they contain almost no values of descent; as expected, both shorter-lived and long-lived ISS occur in air which has ascended. This is consistent with the assumption from *Gierens and Brinkop* [2012] that the descent they found in pdfs of vertical velocity of ISSRs is associated with decaying ISSRs. In winter, the distribution of pressure change for long-lived ISS air has a peak at smaller values of ascent and a smaller variance compared to shorter-lived ISS air (Figure 5b). In summer, the peak of both distributions is similar (Figure 5d), with larger frequencies of strong ascent for the shorter-lived ISS air. Considering the distributions of speed and pressure change together, the slower wind speeds and smaller ascent of long-lived ISS air suggest that it occurs in more slowly evolving weather situations. The rate of change of temperature, pressure, and specific humidity during the period of ice supersaturation is slower in longer-lived ISS trajectories (not shown), which further supports this hypothesis.

[27] Similarly, we can construct pdfs of the direction that the air moved in the 24 h leading up to the first point of ISS, and the 24 h following the first point of ISS, for subsaturated air (the climatology), shorter-lived and long-lived ISS air. Here the results are split by region, to allow for the different synoptic regimes which might influence the flow in each region. Four subregions of interest are defined, based on the spatial distribution of the ISS start points in Figure 3. We refer to these as Atlantic-European, Mid-Atlantic, Greenland, and Iceland; their locations are shown as boxes in Figure 6a. For each region, we consider only those tropospheric ISS trajectories where the first point of ISS is within the region of interest. Winter data are shown for all regions except Iceland, which has a larger number of ISS points in summer.

[28] An example of the movement of air along ISS trajectories is shown in Figure 6 for long-lived tropospheric ISS air which becomes ice supersaturated within the Atlantic-European and Mid-Atlantic regions. The location of these trajectories 24 h prior to becoming ice supersaturated within these regions, and their subsequent location 24 h later, gives an indication of the synoptic conditions in which the ISS occurred. Air which becomes ice supersaturated over the Atlantic-European region comes predominantly from the west and southwest (Figure 6a). However, air which becomes ice supersaturated over the Mid-Atlantic region comes from a westerly direction (Figure 6c) and in general has moved further than air which becomes ice supersaturated over the Atlantic-European region, suggesting the influence of the jet stream. Twenty-four hours after the air becomes ice supersaturated in either region, when it is still supersaturated, it has moved toward the north and east. In the case of persistent contrail formation within these air parcels, contrails which are formed over the region of interest would be

advected toward the north and east, to the regions shown in Figures 6b and 6d. This information can be summarized as pdfs to show the movement of air leading up to and following ISS, for the different regions (Figures 7 and 8).

[29] Pdfs of the direction of movement leading up to ISS are shown in Figure 7. For all regions, the distributions for shorter-lived ISS air are similar to those for subsaturated air, i.e., are similar to climatology. For the Atlantic-European region (Figure 7a) and Mid-Atlantic region (Figure 7b) in winter, which are dominated by the jet stream, flow is predominantly from the west. However, the distribution for longer-lived ISS air shows a higher proportion of southerly winds than subsaturated or shorter-lived ISS air. This is also true for the Iceland region in summer (Figure 7d), where longer-lived ISS air has a higher proportion of flow from the southwest than shorter-lived ISS air. For the Greenland region in winter (Figure 7c), the distribution is broader, meaning that the direction of flow is more variable. This region is generally north of the influence of the jet stream and can have weak upper level flow. For both Greenland and Iceland regions, a greater proportion of the flow comes from an easterly direction.

[30] Further information about the airflows leading to ISS is obtained by considering the direction of flow during the 24 h following the first point of ISS. This is shown for all regions in Figure 8. Once again, the pdfs of direction of movement are similar for subsaturated air and shorter-lived ISS air, indicating that using this method we cannot use flow direction alone to distinguish between subsaturated and short-lived ISS air. For the Atlantic-European and Mid-Atlantic regions (Figures 8a and 8b), for subsaturated and short-lived ISS air, the bulk of the pdf has shifted from flow from the southwest quadrant to flow from the northwest quadrant. However, for long-lived ISS air the peak is from the southwest, indicating that these airflows are still moving north (consistent with Figure 6b) and therefore likely to be experiencing ascent. If we consider instead the direction of flow in the 24 h following the last point of ISS (not shown), we find that the long-lived ISS air now has a northerly component, consistent with the air descending and becoming subsaturated. The difference between short- and long-lived ISS airflows is less clear for the Greenland and Iceland regions, as the variance of the pdfs is large indicating that the flow direction is very variable in these regions.

[31] Put together, these results suggest that ice supersaturation occurs around the northernmost part of the trajectory. This suggests that long-lived ISS air primarily occurs in two different synoptic situations: slower-moving air ascending around the periphery of an anticyclone and air rising in the jet stream circulations (regions of ascent in the right jet entrance and left jet exit) that are on the edge of the circulation rather than in the core of the jet.

4. Conclusions

[32] Ice-supersaturated air parcels have been analyzed using Lagrangian trajectories over the North Atlantic. These highlight the dynamical nature of ice-supersaturated regions that can be readily diagnosed from observational data and meteorological analyses; here we investigate the air which makes up these regions. Trajectories have been calculated from ERA-Interim data for three winter and three summer seasons, giving a large data sample of trajectories which contain ice supersaturation.

[33] The duration of ice supersaturation is generally short lived; the median duration of ISS is less than 6 h for both winter and summer seasons. In winter, the median duration of stratospheric ISS air is longer at 6 h, although this could be an artifact of the coarse time resolution of the meteorological data. Five percent of tropospheric ISS trajectories and 23% of stratospheric ISS trajectories have a duration of at least 24 h. We note that while the partitioning of ISS trajectories into tropospheric and stratospheric has some sensitivity to the tropopause definition, the effect on the distributions of the ISS duration is small. The percentage of ISS air which remains in a supersaturated state for at least 24 h is higher than previous studies of contrail lifetimes [e.g., *Schumann*, 2012]. This is expected, since the duration of ISS air is an upper bound on the lifetime of a contrail forming in that air mass, and loss processes such as sedimentation of ice crystals are not accounted for here. Weighting the ice-supersaturation duration with the observed frequency indicates the likely overall importance of the longer duration ice-supersaturated trajectories, which are a focus of this study.

[34] The evolution of the properties of the air parcel while it is supersaturated shows that air parcels continue to ascend while saturated and lose moisture. The decrease in moisture content could be explained by the formation of cirrus clouds in the ISS air. In this study we have not considered the presence of natural cirrus clouds in the ice-supersaturated air. To do so would require interpolating cloud cover fraction to the location of the trajectories, which could introduce spurious results since cloud cover is not a continuous field. While our results seem to suggest that natural cirrus cloud would eventually form in the majority of air parcels which remain supersaturated for a long period of time, further studies would be required to confirm this. It is adiabatic compression of sinking air parcels rather than loss of moisture which is the major control on the duration of ISS of an air parcel.

[35] We have analyzed the history of air masses to discern differences between subsaturated air and ISS air of short and long duration. For both long- and short-lived ISS, the airflow leading to ice supersaturation is predominantly westerly. However, this turns from having a southerly to northerly component after (the last point of) saturation and only weak ascent. This suggests that the ISS occurs around the northernmost part of the trajectory. In general, long-lived trajectories exhibit different behavior to shorter-lived trajectories; they occur in slower-moving air which is ascending more slowly which implies they are not associated with fast (or the fastest) moving air through a jet stream. The direction of air leading up to ISS also shows a higher proportion of southerly winds than climatology, and the air continues to have a northward component and rise while saturated. However, considering the recent history (the previous 24 h) of short-duration ISS air and subsaturated air, the only difference is that subsaturated air may experience descent in its recent history, whereas short-lived ISS air does not.

[36] Lagrangian trajectories provide a dynamical perspective on ice-supersaturated air and have previously only been used in a case study approach. Here we have extended their use to calculate trajectories for extended periods, to obtain a large sample of trajectories containing ice supersaturation.

The trajectories are useful as an upper bound of the duration of potential contrails forming within ice-supersaturated air parcels; however, they are subject to the limits of the model's capability to represent ice supersaturation. In this study we have not tried to separate out ISS trajectories into different weather situations, to explain the variety of contrail durations. The results of this study suggest that at least long-lived ISS occurs preferentially in some airflows but fails to discern differences between short-lived ISS and subsaturated airflows, beyond confirming that ISS air occurs in rising airflows. These results contribute to a better understanding of the dynamical nature of ice-supersaturated regions which is important for evaluating predictions of ice supersaturation from numerical weather prediction or climate models.

[37] **Acknowledgments.** This work is part of the REACT4C project, funded under the EU 7th framework programme, grant ACP8-GA-2009-233772. The Lagrangian trajectory code was provided by John Methven. We thank Klaus Gierens and John Methven for comments on an earlier draft of the paper. We thank three anonymous reviewers for their comments which helped to improve the manuscript.

References

Barnston, A. G., and R. E. Livezey (1987), Classification, seasonality and persistence of low-frequency atmospheric circulation patterns, *Mon. Weather Rev.*, *115*, 1083–1126.

Burkhardt, U., and B. Kärcher (2011), Global radiative forcing from contrail cirrus, *Nat. Clim. Change*, *1*, 54–58, doi:10.1038/nclimate1068.

Cau, P., J. Methven, and B. J. Hoskins (2005), Representation of dry tropical layers and their origins in ERA-40 data, *J. Geophys. Res.*, *110*, D06110, doi:10.1029/2004JD004928.

Dee, D. P., et al. (2011), The ERA-Interim reanalysis: Configuration and performance of the data assimilation system, *Q. J. R. Meteorol. Soc.*, *137*, 553–597, doi:10.1002/qj.828.

Duda, D. P., P. Minnis, L. Nguyen, and R. Palikonda (2004), A case study of the development of contrail clusters over the Great Lakes, *J. Atmos. Sci.*, *61*, 1132–1146, doi:10.1175/1520-0469(2004)061<1132:ACSOTD>2.0.CO;2.

Gierens, K., and S. Brinkop (2012), Dynamical characteristics of ice supersaturated regions, *Atmos. Chem. Phys.*, *12*, 11,933–11,942, doi:10.5194/acp-12-11933-2012.

Gierens, K., U. Schumann, M. Helten, H. Smit, and A. Marenco (1999), A distribution law for relative humidity in the upper troposphere and lower stratosphere derived from three years of MOZAIC measurements, *Ann. Geophys.*, *17*, 1218–1226, doi:10.1007/s00585-999-1218-7.

Haywood, J. M., R. P. Allan, J. Bornemann, P. M. Forster, P. N. Francis, S. Milton, G. Rädel, A. Rap, K. P. Shine, and R. Thorpe (2009), A case study of the radiative forcing of persistent contrails evolving into contrail-induced cirrus, *J. Geophys. Res.*, *114*, D24201, doi:10.1029/2009JD012650.

Hoose, C., and O. Möhler (2012), Heterogeneous ice nucleation on atmospheric aerosols: A review of results from laboratory experiments, *Atmos. Chem. Phys.*, *12*, 9817–9854, doi:10.5194/acp-12-9817-2012.

Immler, F., R. Treffeisen, D. Engelbart, K. Krüger, and O. Schrems (2008), Cirrus, contrails, and ice supersaturated regions in high pressure systems at northern mid-latitudes, *Atmos. Chem. Phys.*, *8*, 1689–1699, doi:10.5194/acp-8-1689-2008.

Irvine, E. A., B. J. Hoskins, and K. P. Shine (2012), The dependence of contrail formation on the weather pattern and altitude in the North Atlantic, *Geophys. Res. Lett.*, *39*, L12802, doi:10.1029/2012GL051909.

Iwabuchi, H., P. Yang, K. N. Liou, and P. Minnis (2012), Physical and optical properties of persistent contrails: Climatology and interpretation, *J. Geophys. Res.*, *117*, D06215, doi:10.1029/2011JD017020.

Jackson, D. R., J. Methven, and V. Pope (2001), Transport in the low latitude tropopause zone diagnosed using particle trajectories, *J. Atmos. Sci.*, *58*, 173–192.

Kästner, M., R. Meyer, and P. Wendling (1999), Influence of weather conditions on the distribution of persistent contrails, *Meteorol. Appl.*, *6*, 261–271.

Lamquin, N., C. J. Stubenrauch, K. Gierens, U. Burkhardt, and H. Smit (2012), A global climatology of upper-tropospheric ice supersaturation occurrence inferred from the Atmospheric Infrared Sounder calibrated by MOZAIC, *Atmos. Chem. Phys.*, *12*, 381–405, doi:10.5194/acp-12-381-2012.

Lee, D. S., D. W. Fahey, P. M. Forster, P. J. Newton, R. C. N. Wit, L. L. Lim, B. Owen, and R. Sausen (2009), Aviation and global climate change in the 21st century, *Atmos. Environ.*, *43*, 3520–3537, doi:10.1016/j.atmosenv.2009.04.024.

Methven, J. (1997), Offline trajectories: Calculation and accuracy, *Tech. Rep. 44*, 18 pp., U. K. Univ. Global Atmos. Modelling Programme, Dept. of Meteorol., Univ. of Reading, Reading, U. K.

Methven, J., S. R. Arnold, F. M. O'Connor, H. Barjat, K. Dewey, J. Kent, and N. Brough (2003), Estimating photochemically produced ozone throughout a domain using flight data and a Lagrangian model, *J. Geophys. Res.*, *108*(D9), 4271, doi:10.1029/2002JD002955.

Minnis, P., D. F. Young, D. P. Garber, L. Nguyen, W. L. Smith Jr., and R. Palikonda (1998), Transformation of contrails into cirrus during SUCCESS, *Geophys. Res. Lett.*, *25*, 1157–1160, doi:10.1029/97GL03314.

Montoux, N., P. Keckhut, A. Hauchecorne, J. Jumelet, H. Brogniez, and C. David (2010), Isentropic modeling of a cirrus cloud event observed in the midlatitude upper troposphere and lower stratosphere, *J. Geophys. Res.*, *115*, D02202, doi:10.1029/2009JD011981.

Pruppacher, H. R., and J. D. Klett (1997), *Microphysics of Clouds and Precipitation*, Atmospheric and Oceanographic Sciences Library, Kluwer Acad., Dordrecht, The Netherlands.

Schumann, U. (2012), A contrail cirrus prediction model, *Geosci. Model Dev.*, *5*, 543–580, doi:10.5194/gmd-5-543-2012.

Spichtinger, P., K. Gierens, and W. Read (2003), The global distribution of ice-supersaturated regions as seen by the Microwave Limb Sounder, *Q. J. R. Meteorol. Soc.*, *129*, 3391–3410, doi:10.1256/qj.02.141.

Spichtinger, P., K. Gierens, and H. Wernli (2005a), A case study on the formation and evolution of ice supersaturation in the vicinity of a warm conveyor belt's outflow region, *Atmos. Chem. Phys.*, *5*, 973–987, doi:10.5194/acp-5-973-2005.

Spichtinger, P., K. Gierens, and A. Dörnbrack (2005b), Formation of ice supersaturation by mesoscale gravity waves, *Atmos. Chem. Phys.*, *5*, 1243–1255, doi:10.5194/acp-5-1243-2005.

Tiedtke, M. (1993), Representation of clouds in large scale models, *Mon. Weather Rev.*, *121*, 3040–3061.

Tompkins, A. M., K. Gierens, and G. Rädel (2007), Ice supersaturation in the ECMWF integrated forecast system, *Q. J. R. Meteorol. Soc.*, *133*, 53–63, doi:10.1002/qj.14.

Vazquez-Navarro, M. R. (2009), Life cycle of contrails from a time series of geostationary satellite images, PhD thesis, Deutsches Zentrum für Luft und Raumfahrt.

Voigt, C., et al. (2010), In-situ observations of young contrails—Overview and selected results from the CONCERT campaign, *Atmos. Chem. Phys.*, *10*, 9039–9056, doi:10.5194/acp-10-9039-2010.

Zängl, G., and K. P. Hoinka (2001), The tropopause in the Polar regions, *J. Clim.*, *14*, 3117–3139, doi:10.1175/1520-0442(2001)014.